Geophys. J. Int. (2005) **160,** 804–814 doi: 10.1111/j.1365-246X.2005.02527.x

Interpretation of two-dimensional magnetotelluric profile data with three-dimensional inversion: synthetic examples

Weerachai Siripunvaraporn,[1] Gary Egbert[2] and Makoto Uyeshima[3]

[1]*Department of Physics, Faculty of Science, Mahidol University, Rama VI Rd, Rachatawee, Bangkok,* 10400, *Thailand. E-mail: scwsp@mahidol.ac.th*
[2]*College of Oceanic and Atmospheric Science, Oregon State University, Corvallis,* OR 97331, *USA. E-mail: egbert@coas.oregonstate.edu*
[3]*Earthquake Research Institute, University of Tokyo,* 1-1-1 *Yayoi, Bunkyo-ku, Tokyo* 113-0032, *Japan. E-mail: Uyeshima@eri.u-tokyo.ac.jp*

Accepted 2004 November 15. Received 2004 November 11; in original form 2004 July 20

SUMMARY

Traditional methods for interpretation of magnetotelluric (MT) profile data are based on 2-D inversion, under the assumption that 3-D complications in the data can be treated as 'geological noise'. We show with synthetic models that fitting 3-D data with a 2-D inversion can result in spurious features, especially if transverse electric (TE) data are used. Inversion of a single profile of MT data with a 3-D algorithm results in significantly more realistic images of structure beneath the data profile, and also allows some resolution of nearby off-profile structure. We also consider the importance of including the on-diagonal impedance tensor terms, $\boldsymbol{Z}_{xx}$ and $\boldsymbol{Z}_{yy}$, in the inversion. In synthetic test cases, fitting these diagonals improves the accuracy of images of off-profile structure, particularly near the edge of a conductive feature.

Key words: 3-D effects, 3-D inversion, electromagnetic induction, magnetotellurics.

1 INTRODUCTION

In most cases, magnetotelluric (MT) data are still collected on 2-D profiles across an assumed geoelectrical strike. The strike is typically chosen prior to data acquisition, based on the trend of a coastline, known faults (e.g. Unsworth *et al.* 2000) or other regional structures (e.g. Sakkas *et al.* 2002; Wu *et al.* 2002; Brasse *et al.* 2002). After data collection and processing, various techniques such as the Groom–Bailey (Groom & Bailey 1989) or other tensor decomposition (e.g. Chave & Smith 1994; Caldwell *et al.* 2004), induction arrow plots (Parkinson 1959,) and skews (Swift 1967; Vozoff 1972) are used to check (and sometimes refine) assumptions about dimensionality or geoelectrical strike (e.g. Ogawa *et al.* 2001; Mitsuhata *et al.* 2001; Sakkas *et al.* 2002; Pous *et al.* 2002; Bai & Meju 2003; Bielinski *et al.* 2003). Once the geoelectrical strike has been determined, impedances are rotated into the strike direction, and the off-diagonal impedances (or transverse electric (TE) and transverse magnetic (TM) apparent resistivities and phases) are fitted with a 2-D inversion (e.g. deGroot-Hedlin & Constable 1990; Smith & Booker 1991; Ogawa & Uchida 1996; Siripunvaraporn & Egbert 2000; Rodi & Mackie 2001) to generate cross-sections of electrical resistivity.

In reality, the assumption that the data are purely, or even almost, 2-D seldom holds over the full range of periods used. Off-profile (i.e. 3-D) structures affect most data sets to at least some degree (e.g. Brasse *et al.* 2002). In trying to fit such data with a 2-D inversion, there is a significant danger of introducing spurious structure or unrealistic resistivity values beneath the profile, especially as data misfits are reduced. Most researchers are well aware of these potential pitfalls to 2-D interpretation, and are careful to state their conclusions with due caution. But deciding how well to fit a given data set with a 2-D model, and which of the features in the resulting conductivity images are robust, remains a serious challenge in the interpretation of MT data.

Many previous publications (e.g. Wanamaker *et al.* 1984; Berdichevsky *et al.* 1998; Ledo *et al.* 2002) have considered some of the limitations of 2-D interpretation of 3-D MT data using the techniques outlined above. Although we touch on this issue briefly here, our primary goal in this paper is to demonstrate the value of applying a 3-D inversion algorithm to interpretation of individual MT profiles. Using synthetic data generated from a simple 3-D model, we show that inverting MT profile data with a 3-D inversion helps avoid contamination by off-plane structures. Cross-sections of resistivity beneath and near the profile reflect more closely the model used to generate the synthetic data than those obtained with 2-D inversions. In addition, we also consider the importance of including the diagonal impedance elements $\boldsymbol{Z}_{xx}$ and $\boldsymbol{Z}_{yy}$ in the 3-D inversion. These terms are strongly affected by off-profiles structures, so including these leads to a more reasonable model near the data transect, especially if there are significant off-profile structures nearby.

2 TEST MODEL AND SYNTHETIC DATA

The test model (Fig. 1) consists of a 1 Ω m conductive block of dimension 4 km × 2 km × 1 km inside a 100 Ω m host. Here we consider two cases, with the conductor buried from 800 m to 1.8 km depth (model BC; buried conductor) and with the conductor

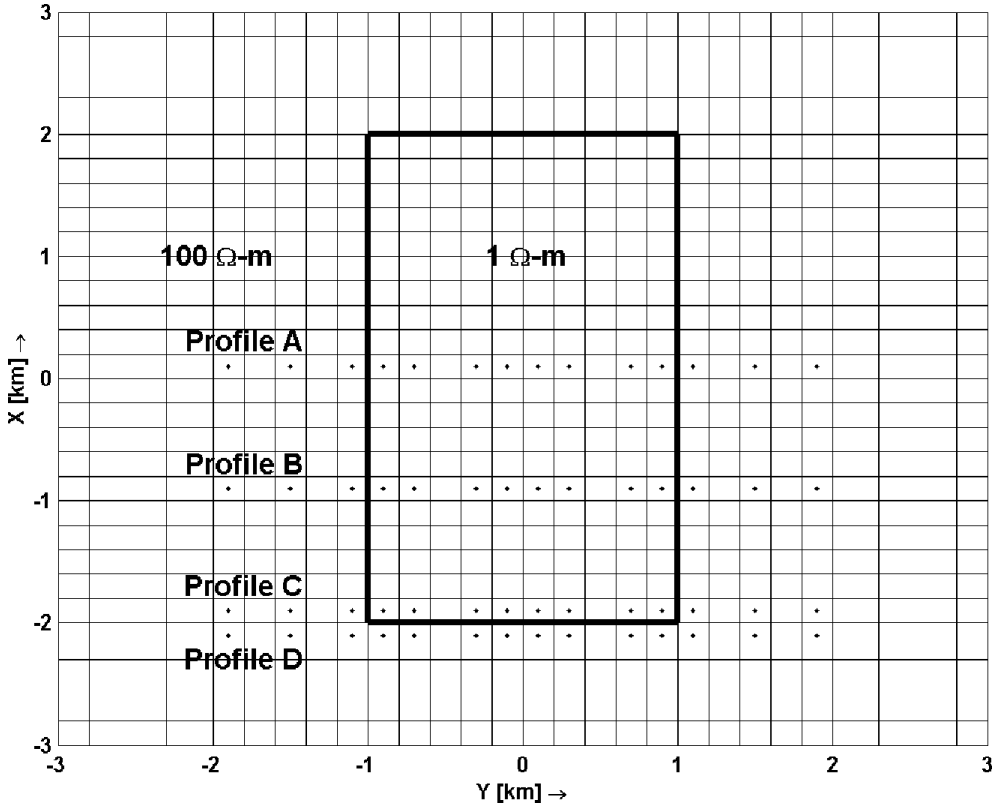

Figure 1. Plan view of the synthetic model used to generate MT data on four profiles, labelled A, B, C and D. The solid dots indicate the data sites. The dominant geoelectric strike is in the *x* direction. Two models are considered: one with a 1 km thick conductor exposed at the surface (model SC), and one with the conductor buried from 800 m to 1.8 km depth (model BC).

exposed at the surface (model SC; surface conductor). Both models are discretized on a 38 × 36 × 30-layer (+7 air layers) grid. Four profiles (A, B, C and D), shown as solid dots in Fig. 1, are considered. Profile A cuts nearly across the middle of the conductive block, while profile B is located midway between the centre and the southern edge of the conductive block. Profiles C and D are located 100 m on either side of the southern Edge of the block. Complex impedance tensors ($\boldsymbol{Z}_{xx}$, $\boldsymbol{Z}_{xy}$, $\boldsymbol{Z}_{yx}$ and $\boldsymbol{Z}_{yy}$) were generated for all profiles at 18 sites and 12 periods (0.001, 0.003, 0.010, 0.031, 0.100, 0.316, 1.000, 3.160, 10.000, 31.600, 100.000 and 316.000 s) using a 3-D forward modelling code of Siripunvaraporn *et al.* (2002). Gaussian noise, with an amplitude of 5 per cent of $|\boldsymbol{Z}_{xy}\boldsymbol{Z}_{yx}|^{1/2}$ was added to the synthetic data. In addition, to simulate the 2-D case, we consider profile O computed for a conductive block of infinite north–south extent. Profile O will be used as a control data set for comparison with other profiles. For 2-D inversion tests the off-diagonal impedance components for all profiles were converted into apparent resistivities and phases in the usual way.

The noise-free apparent resistivities and phases are shown in Figs 2 and 3, and pseudo-sections of the diagonal impedance components, $\boldsymbol{Z}_{xx}$ and $\boldsymbol{Z}_{yy}$, are shown in Figs 4 and 5. Edge effects due to truncation of the conductor can be clearly seen at most periods in the diagonal terms, $\boldsymbol{Z}_{xx}$ and $\boldsymbol{Z}_{yy}$, especially for profiles B, C and D in both models (Figs 4 and 5). Even though profile A is located almost in the middle of the conductor, these edge effects can also be observed (Figs 4 and 5), but magnitudes are much lower than those of other profiles. The edge of the conductor is more clearly evident for case SC where the conductor extends to the surface than for case BC where the conductor is buried. Thus, we may anticipate that edge effects will be less important for the case of a buried conductor.

Figs 2 and 3 show apparent resistivities and phases for the *yx* polarization (i.e. the TM mode for the 2-D case; third and fourth rows of Figs 2 and 3). These are quite similar for profiles O, A, B and even C at almost all periods. However, for the *xy* polarization (the TE mode for the 2-D case; first and second rows of Figs 2 and 3), results are similar only for shorter periods. This shows that truncation of the conductor in our simple models affects the *xy* polarization strongly, but has minimal effects on the *yx* polarization, consistent with the observations of Wanamaker *et al.* (1984) and many others since (but see Berdichevsky *et al.* 1998 for further discussion).

3 NUMERICAL INVERSION EXPERIMENTS AND DISCUSSIONS

Our goal in this paper is to demonstrate the application of a 3-D inversion algorithm to a single MT profile crossing an elongated structure of finite length. We do not consider issues of dimensionality or strike analysis, topics which have been discussed in numerous previous publications (e.g. Ledo *et al.* 2002; Brasse *et al.* 2002, among others). In this paper, we first apply a 2-D inversion to all profiles of both models BC and SC assuming that we know *a priori* that the geoelectric strike is north–south, so $\boldsymbol{Z}_{xy}$ and $\boldsymbol{Z}_{yx}$ are the nominal TE and TM mode impedances respectively. We then apply a 3-D inversion to all profiles of both models using all complex impedance tensor terms. Finally we consider

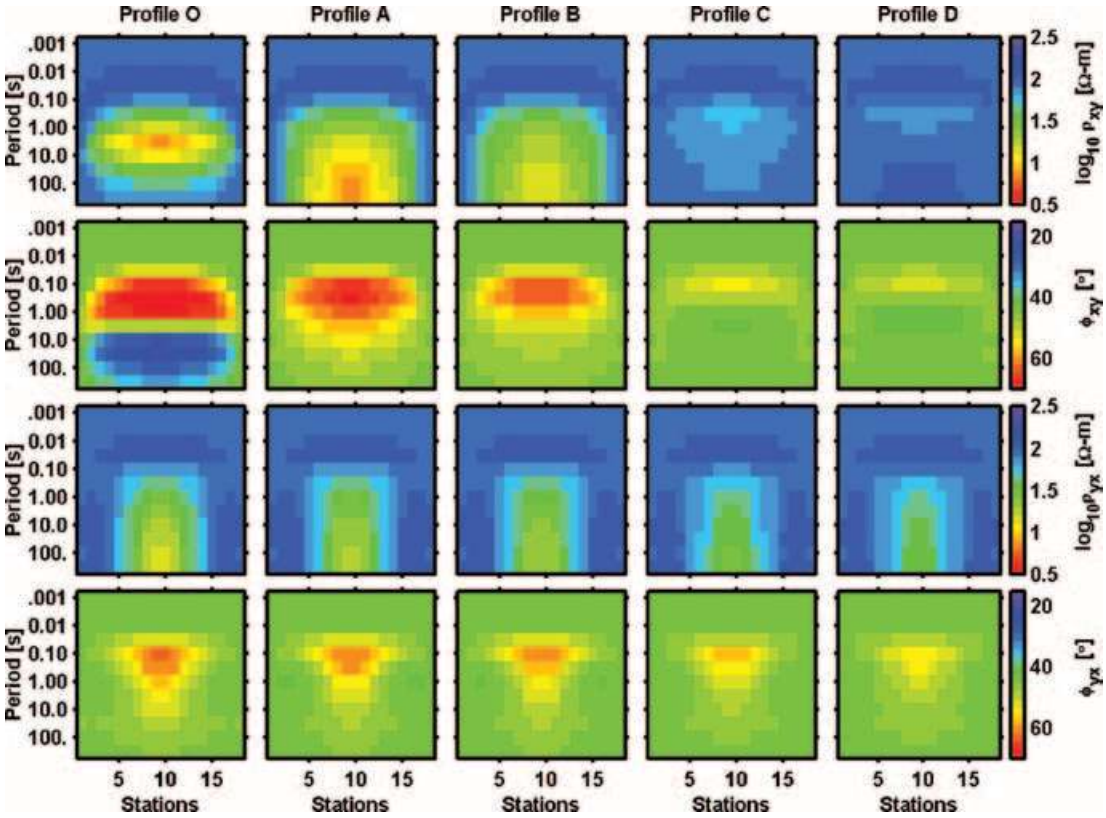

Figure 2. Apparent resistivities and phase pseudo-sections computed from $\boldsymbol{Z}_{xy}$ and $\boldsymbol{Z}_{yx}$ for each profile of model BC. From left to right data are plotted for profiles O, A, B, C and D, respectively. From top to bottom are $\log_{10}\rho_{xy}$, ϕ_{xy}, $\log_{10}\rho_{yx}$, ϕ_{yx}, respectively. The horizontal axis indicates the station number from west to east (y direction), and the vertical axis indicates period.

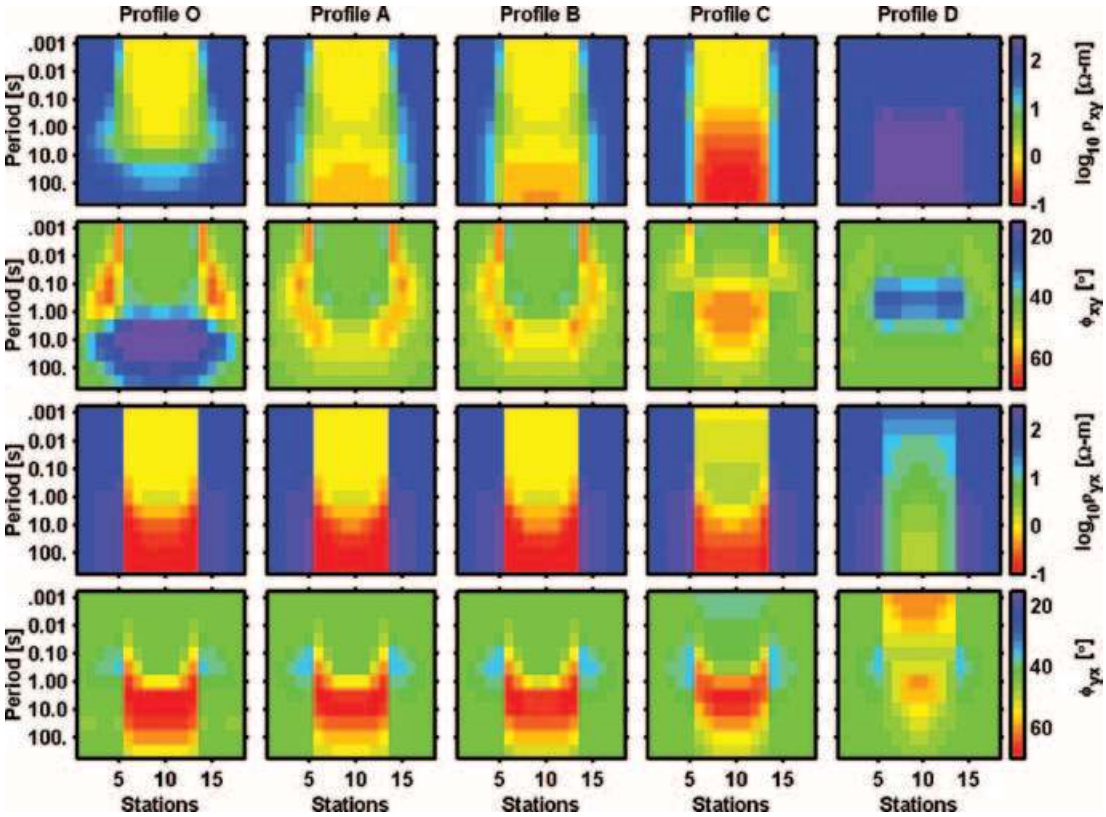

Figure 3. Apparent resistivities and phase pseudo-sections for each profile of model SC, with plotting conventions as in Fig. 2. Note that the colour scales for apparent resistivity differ from Fig. 2.

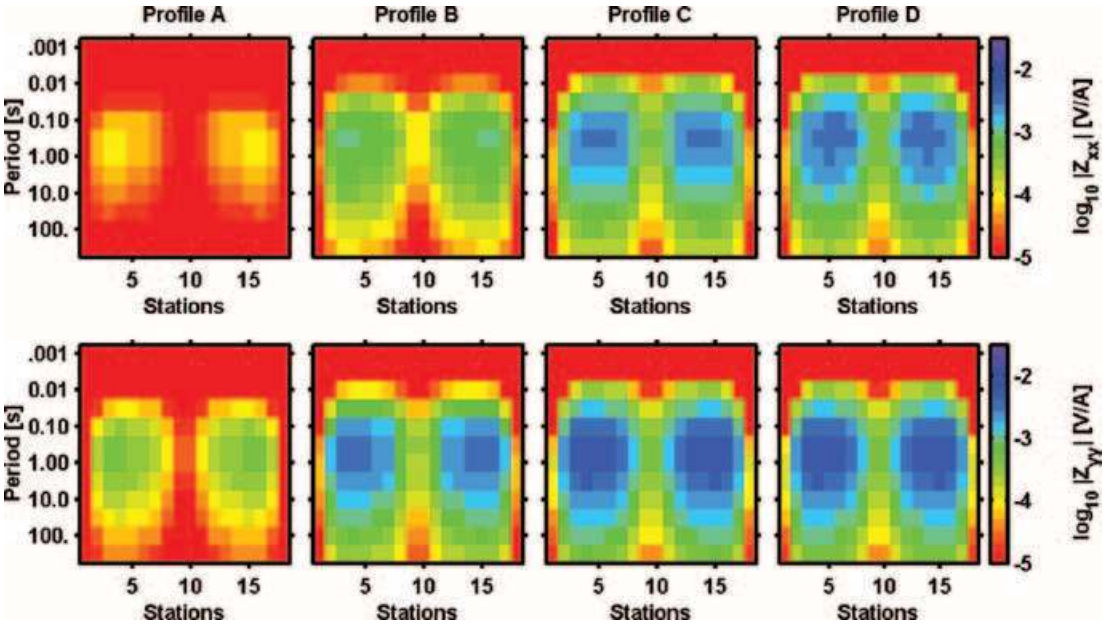

Figure 4. Diagonal impedance tensor terms, $\boldsymbol{Z}_{xx}$ and $\boldsymbol{Z}_{yy}$, generated from model BC. Left to right are results for profiles A, B, C and D, respectively. The upper row is log10 $|\boldsymbol{Z}_{xx}|$ and the lower row is log10 $|\boldsymbol{Z}_{yy}|$. The horizontal axis indicates station number from west to east (y direction), and the vertical axis period.

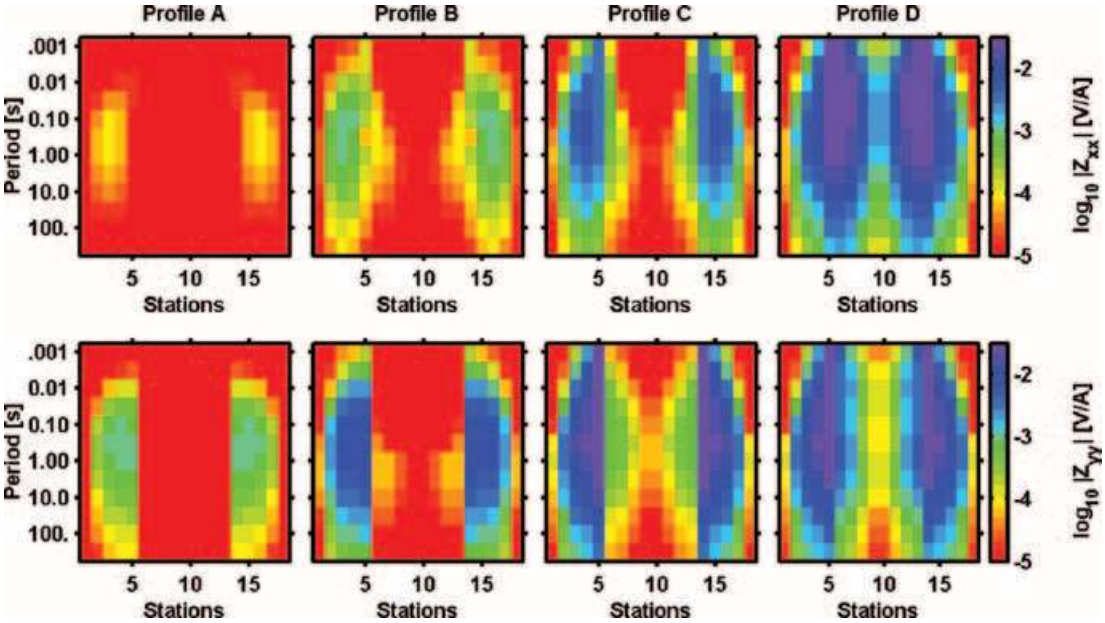

Figure 5. As in Fig. 4, but from model SC.

3-D inversion using only the off-diagonal terms used for the 2-D inversion.

3.1 2-D inversion results

For the 2-D inversion we used the REBOCC code described in Siripunvaraporn & Egbert (2000). This inversion is essentially a data space variant of the OCCAM scheme of Constable *et al.* (1987) and deGroot-Hedlin & Constable (1990), which finds a minimum norm solution subject to fitting data to within a specified tolerance. All inversions were started from a 50 Ω m homogeneous half-space. Data errors are assumed to be 5 per cent, as used for generating the synthetic data. Results of the 2-D inversions of models BC and SC are shown in Figs 6 and 7, respectively, for profiles O, A, B, C and D from top to bottom. Columns from left to right give results of inverting only the TE data (amplitude and phase), only the TM data, and jointly inverting both TM and TE data, respectively.

For the purely 2-D data set (profile O) the 2-D inversion scheme performs well for TE, TM and joint inversion for both models (first row of Figs 6 and 7). In all cases the inversion has no difficulty in retrieving the structure and fitting the data to within a normalized RMS of 1. For data generated from model BC, TM inversions can reduce the normalized RMS misfit to below 2 for profiles A and B, and to 1 for profiles C and D near the conductor's edge. For

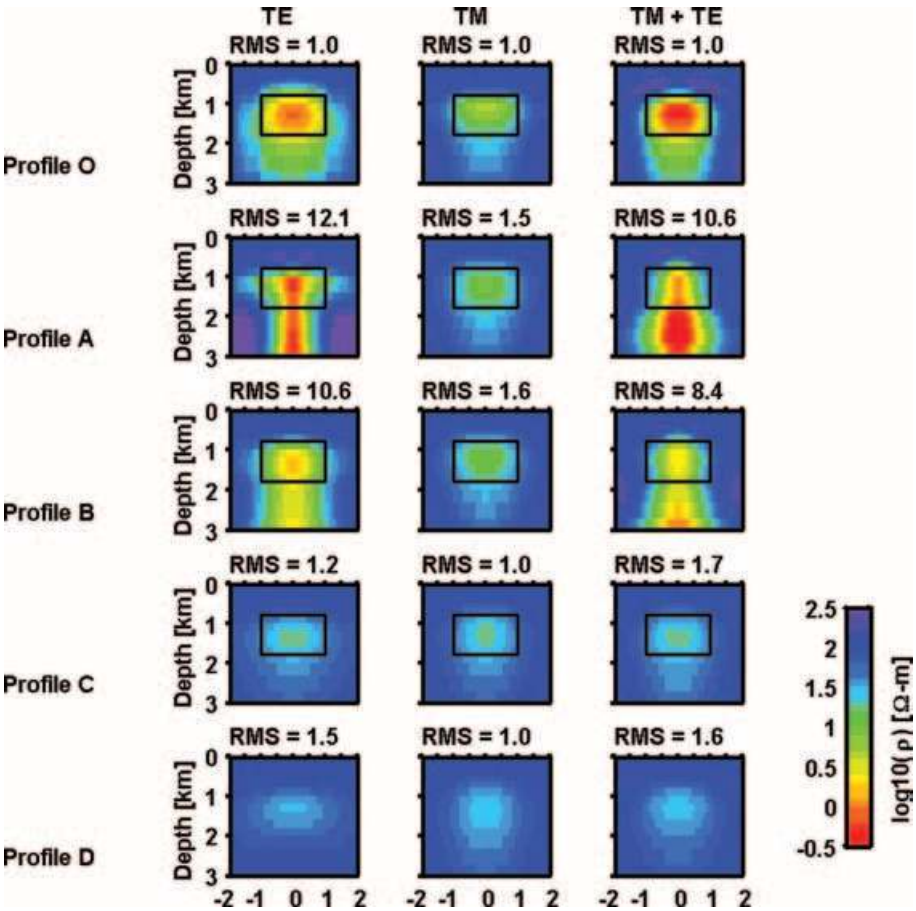

Figure 6. Resistivity cross-sections from 2-D inversion of data generated from model BC on profiles O, A, B, C and D, from top to bottom respectively. The first column gives results for inversion of only TE data, the middle column for only TM data and the last column for joint inversion of TM and TE data. The rectangle outlines the conductor in the synthetic model.

model SC where the conductor is exposed, an RMS misfit of 1 can be achieved for all profiles. Inverting only the TM mode generates a reasonable resistivity structure for most profiles (middle column of Fig. 7). This confirms results from a number of previous studies which have shown that TM mode data are least affected by 3-D effects (Wanamaker *et al.* 1984; Ledo *et al.* 2002). However, the true resistivity contrast is underestimated somewhat, especially for profiles near the edge. When the conductor is buried (model BC), models obtained by inverting only TM mode data show a conductor in the right area but with a resistivity about 10 times too high, approaching the host resistivity. This tendency to underestimate the resistivity contrast becomes more severe as the profile is moved closer to the end of the conductive feature.

The TE and joint TM + TE 2-D inversions do not perform well for either of the 3-D test cases (first and third columns of Figs 6 and 7). In no case is the desired normalized RMS misfit of 1 achieved. The inverse solutions from TE and joint TE and TM inversions of profiles A and B do contain conductive features in the general area of the conductor for both test cases. However, the size and shape of this structure is poorly resolved. For model BC the imaged conductive root extends to greater depth, and in model SC resistivities are unreasonably low (less than 0.1 Ω m). Similar extremely low resistivities are often encountered in 2-D inversion results with real data, and are clearly an artefact of over-fitting the data.

For profiles C and D of model BC, the effects from the conductor are weak, as seen in the similarity of TE responses from these two profiles (Fig. 2). The solutions resulting from TE and joint TM + TE 2-D inversions are therefore almost the same (Fig. 6) and data fits are reasonable. In contrast, for model SC, where the responses for the two profiles differ significantly, the inverse solutions show conductive features in profile C and resistive features in profile D, as they should. However, spurious high- and low-resistivity regions can be seen in the inversion results for both profiles, and the data fits are now poor.

The biggest misfits in the TE and joint 2-D inversions are due to 3-D effects at longer periods. To fit the long-period data better, the inversion extends the conductive root deeper for model BC and reduces resistivities for model SC to an extremely low level. This failure is not specific to REBOCC, or any other 2-D inversion scheme. Almost certainly no 2-D model exists which can fit these 3-D data sets to a target RMS of 1. In this circumstance, deciding how well data should in fact be fitted in a 2-D inversion is problematic, especially since over-fitting the data even a little can result in spurious and poorly resolved structures in the inverse solutions. Most seriously these spurious features may appear to be at least physically sensible in some cases, and thus be erroneously interpreted as real geological structures.

3.2 3-D inversion results: all complex tensor terms

We will now show that by inverting single profile data with a 3-D inversion program, many of the problems encountered with a 2-D

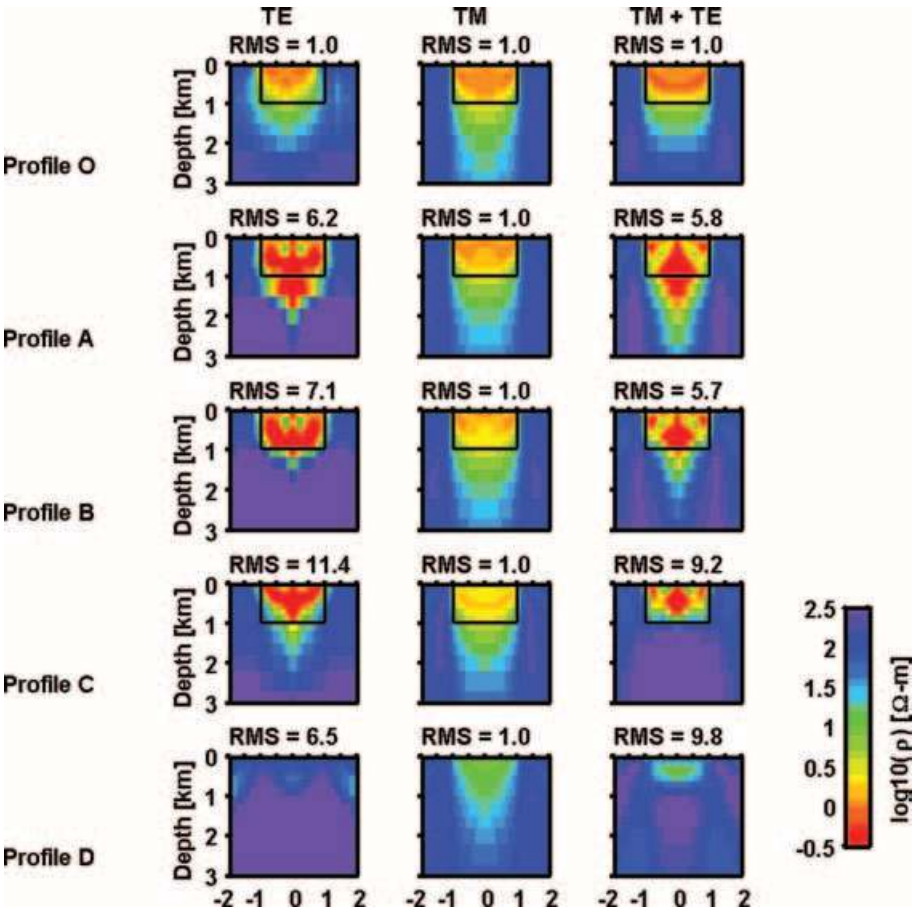

Figure 7. As in Fig. 6, but for model SC.

approach can be significantly reduced, and the data can be fitted with a reasonable model. We first invert the synthetic data from each profile with the 3-D inversion program of Siripunvaraporn *et al.* (2005), using all complex tensor terms, i.e. $\boldsymbol{Z}_{xx}$, $\boldsymbol{Z}_{xy}$, $\boldsymbol{Z}_{yx}$ and $\boldsymbol{Z}_{yy}$. The 3-D inversion code is similar to the 2-D code in that it is a data space variant on the OCCAM minimum structure approach. Results of applying this inversion to the synthetic data discussed above are shown in Fig. 8 for model BC and Fig. 9 for model SC. Inverse solution cross-sections directly beneath each profile are shown in the middle (fourth) column, with solution cross-sections for profiles 1 km, 0.6 km and 0.2 km south, and 0.2 km, 0.6 km and 1 km north of the data transect shown in the first, second, third, fifth, sixth and seventh columns, respectively. In most cases data are readily fitted to a normalized RMS of 1. One exception is for profile C of model SC, where the inversion was only able to reduce the normalized RMS misfit to about 1.8.

For the 3-D inversions cross-sections directly beneath the data profile are always reasonably consistent with the true model used to generate the synthetic data, although the shape and resistivity are distorted to varying degrees. The most serious deficiency is in the inverse solutions for the buried conductor (model BC) where the conductivity contrast is systematically reduced. This bias almost certainly results primarily from the minimum norm formulation of the inverse problem, which trades off between minimizing conductivity variations and data misfit. When the effect of a structure on the data is weak, as for the buried conductor, conductivity contrasts that are systematically too small are favoured because these keep the model norm small, with little increase in data misfit. Improved data coverage (i.e. additional profiles) may improve accurate resolution of the conductive anomaly (Siripunvaraporn *et al.* 2005). Different approaches to regularization of the inverse problem may possibly also improve results.

The bias toward low resistivity contrasts for buried structures is even more severe when only TM mode data are inverted with a 2-D approach (Fig. 6). Inclusion of data for both source polarizations in the 3-D inversion evidently improves accuracy of the estimated contrast. As we have seen, trying to include data from this second polarization in a 2-D inversion can lead to very poor results. These problems are not seen in the 3-D inversion results (Figs 8 and 9). The 2-D inversion inserts spurious structures such as deepened conductive roots (Fig. 6) or unrealistic resistivities (Fig. 7) beneath the profile in an effort to account for 3-D features in the long-period data. For the 3-D inversion these 3-D effects can be accounted for more reasonably with actual off-profile structure. In the simple case of model SC where the conductor is exposed to the surface, inverting only TM mode data generates a reasonable model, and one might argue that a 3-D inversion is unnecessary. However, real data sets are generally affected by both deep and shallow structures, and some of these are likely to be very poorly resolved using only TM mode data. As a consequence most interpretations of MT field surveys incorporate TE mode data to some degree. By reducing the weight given to fitting these data some of the spurious effects seen in our examples can probably be reduced, but one can never be certain that they have been completely eliminated.

Using a 3-D inversion allows use of all of the data to image the structure beneath the data profile, with much less risk of introducing spurious structure, but how good are the images of off-profile

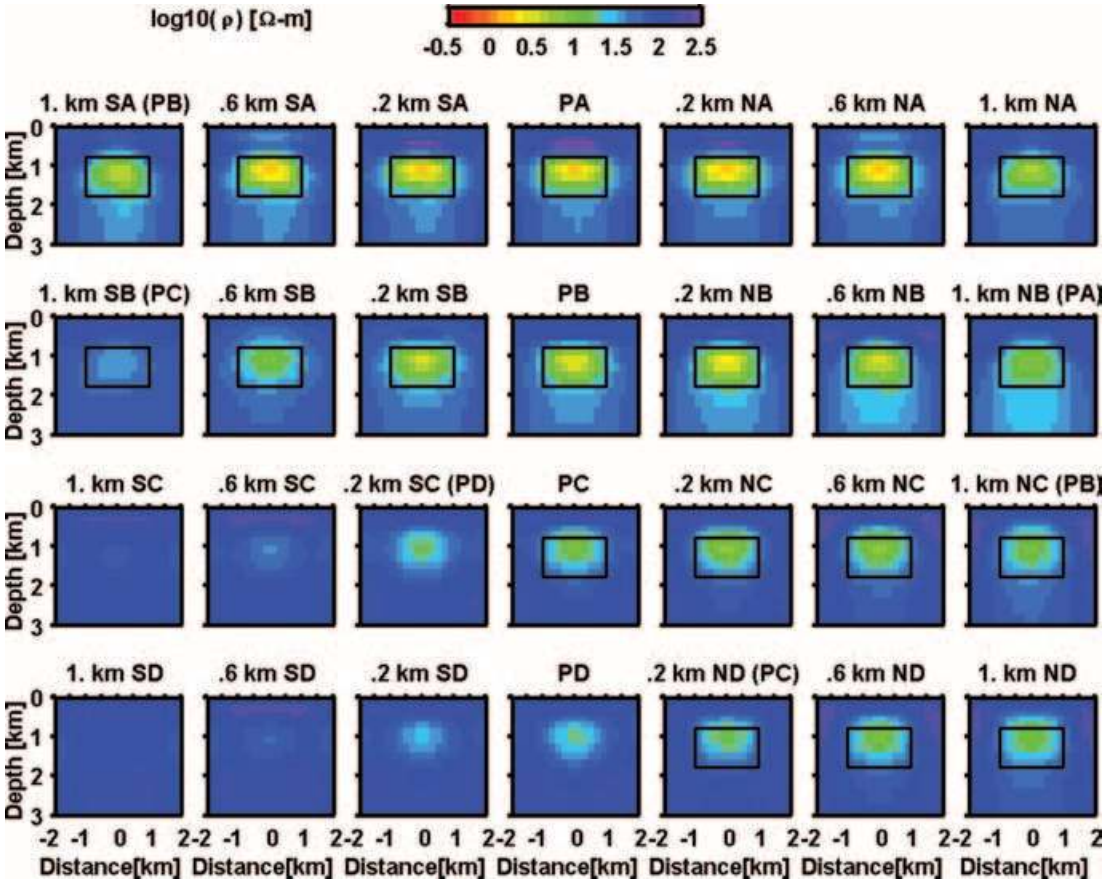

Figure 8. Resistivity cross-sections from 3-D inversion of all complex impedance tensor elements generated from model BC. From top to bottom are sections of the 3-D inverse solutions of data from profiles A, B, C and D, respectively. The centre column (fourth) shows the cross-section directly beneath each profile, PA, PB, PC and PD. The left (first, second, third) and right (fifth, sixth, seventh) columns show the models from 1 km, 600 m and 200 m south (SA, SB, SC and SD) and 200 m, 600 m and 1 km north (NA, NB, NC and ND) of the profile. The rectangle outlines the conductor.

structure? For 3-D inversion of data from profile A (first row of Figs 8 and 9), the imaged conductor continues for almost 1 km to the north and south. For the profile B inversion the conductor extends a similar distance to the north, and somewhat less to the south. In all cases for profiles A and B, the imaged conductor is shorter than the true structure. This again can be explained in terms of biases in a minimum norm solution. Structures more than about 1 km from the profile have limited effect on, and are thus not required by, the data.

For profiles C and D which are closer to the edge of the conductor the value of 3-D inversion of profile data is demonstrated even more clearly. For profile C, which is 100 m inside the southern edge of the conductor, the 3-D inversion shows a conductor beneath, and to the north of, the profile, but conductivity diminishes rapidly to the south for both models (third row of Figs 8 and 9). For profile D, which is located 100 m outside the southern edge of the conductor, the 3-D inversion shows little increase in conductivity beneath, and south of, the profile. However, the conductor is clearly displayed north of the profile, in roughly the correct location (fourth row of Figs 8 and 9). Thus, the edge of the conductor is reasonably recovered using profile data from either side, especially for the case of near-surface structure (Fig. 9, last two rows).

As discussed above, for the buried conductor responses on profiles C and D are quite similar. Not surprisingly, results of 3-D inversion for these profiles are also similar (third and fourth rows of Fig. 8), and the edge of the conductor is less clearly seen. Also, because the data on these edge profiles are only weakly affected by the conductor, resistivity contrasts resulting from these inversions are especially weak. Nevertheless, the 3-D inversion using all complex tensor elements still produces a qualitatively correct picture of a buried conductor extending northward (but not southward) from near profiles C and D.

Obviously information about off-profile structure that can be recovered from a single profile of MT data is limited. The results of 3-D inversion should clearly be interpreted cautiously, particularly with regard to the along-strike extent of structures. However, reasonable images can be obtained for structures beneath, and near, a single MT profile, while even this type of information cannot be obtained reliably with 2-D inversion.

3.3 3-D inversion results: inverting only Z_{xy} and Z_{yx}

In the examples considered above we inverted all four impedance tensor components, $\boldsymbol{Z}_{xx}$, $\boldsymbol{Z}_{xy}$, $\boldsymbol{Z}_{yx}$ and $\boldsymbol{Z}_{yy}$. Now we consider inversion of only the off-diagonal terms $\boldsymbol{Z}_{xy}$ and $\boldsymbol{Z}_{yx}$, comparable to a joint TE + TM 2-D inversion. Results are shown in Figs 10 and 11 for models BC and SC, respectively. The first point to note is that even though fewer data are used the inversion algorithm more frequently fails to reach the desired RMS of 1, especially for model

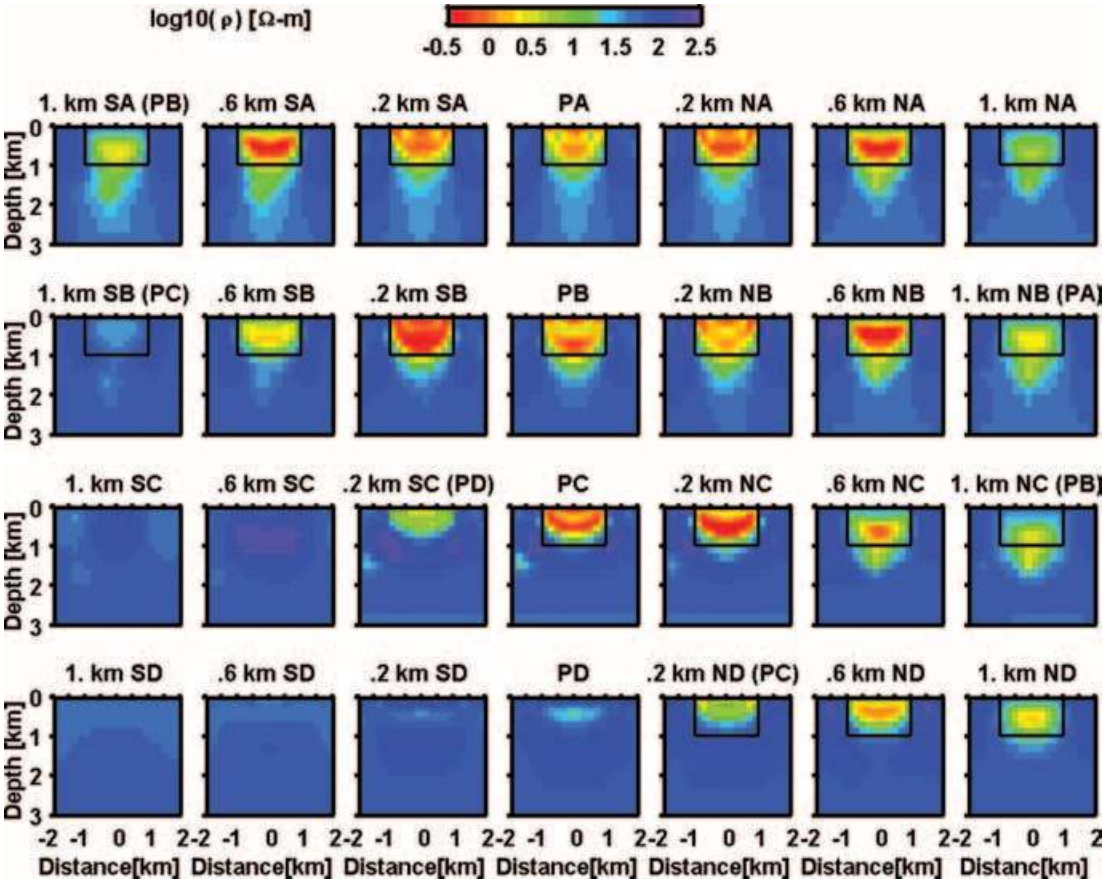

Figure 9. Resistivity cross-sections as in Fig. 8, but for data from model SC.

SC. The inverse solutions shown in Figs 10 and 11 achieved the minimum RMS misfit, which were for profiles A, B, C and D respectively, 1.25, 1.00, 1.00 and 1.00 for model BC, and 1.38, 1.10, 2.60 and 1.40, for model SC.

Similar to the inverse solutions in Figs 8 and 9, obtained using all tensor components, cross-sections directly beneath the MT profiles are in fair agreement with the true model, though the conductor's shape and size are slightly distorted (Figs 10 and 11). The extremely low resistivity values or deep conductor roots, seen when the same data were fitted with a 2-D inversion, are not seen here. This again clearly demonstrates the benefit of 3-D inversion of single-profile MT data. For profiles A and B, and for both models, the conductor in the inverse solutions continues to both north and south (first and second rows of Figs 10 and 11), as in the full impedance inversion results.

Greater differences between the full tensor and off-diagonal cases are seen for profiles C and D. Without $\boldsymbol{Z}_{xx}$ and $\boldsymbol{Z}_{yy}$, the conductor is barely seen in model BC (third and fourth rows of Fig. 10), but appears continuously both north and south of the profiles in model SC (third and fourth rows of Fig. 11), though in this case the conductor is significantly reduced and shallower for profile D. The edge of the conductor is also lost in both models. This indicates that significant information about the conductor's edge is clearly present in the on-diagonal tensor elements, $\boldsymbol{Z}_{xx}$ and $\boldsymbol{Z}_{yy}$. Without this information, the data do not distinguish between directions off profile.

Indeed, consider a profile the same distance to the north of the conductor as D is to the south. The off-diagonal tensor components, $\boldsymbol{Z}_{xy}$ and $\boldsymbol{Z}_{yx}$ would be the same as on D, but the diagonal tensor components $\boldsymbol{Z}_{xx}$ and $\boldsymbol{Z}_{yy}$ would have the opposite sign. Hence from off-diagonal components alone one could not determine on which side of the profile the conductive layer is; this information is only in the sign of the diagonal components.

Symmetry considerations also show that for any 3-D conductivity that is symmetric about the profile (in particular for the uniform conductivity Earth used as the starting model in our inversion) data sensitivities for the off-diagonal impedances will also be symmetric about the profile. This symmetry in sensitivities for the reduced data set may help explain why the inversion search algorithm fails to find a model which fits the data at the target misfit. Starting from a symmetric conductivity distribution, all data sensitivities (and for an Occam-style inversion approach, all model updates) should remain symmetric about the profile if only off-diagonal impedances are used. Models which fit the off-diagonal data adequately exist, but these are presumably all asymmetric, in contrast to the symmetric models that should result from a linearized search of the sort we use. It is interesting to note that this provides a simple example of a situation in which a linearized search may fail to converge to the global minimum of the penalty functional.

In fact, the models from inversion of only off-diagonal impedances from profiles C and D are nearly, but not exactly, symmetric (Figs 10 and 11). The symmetry in the sensitivity calculation is broken, both by numerical truncation error and due to some technical details in the approximate way in which we have implemented the model covariances (Siripunvaraporn & Egbert 2000). This breaking in symmetry could help the inversion find models that fit the data

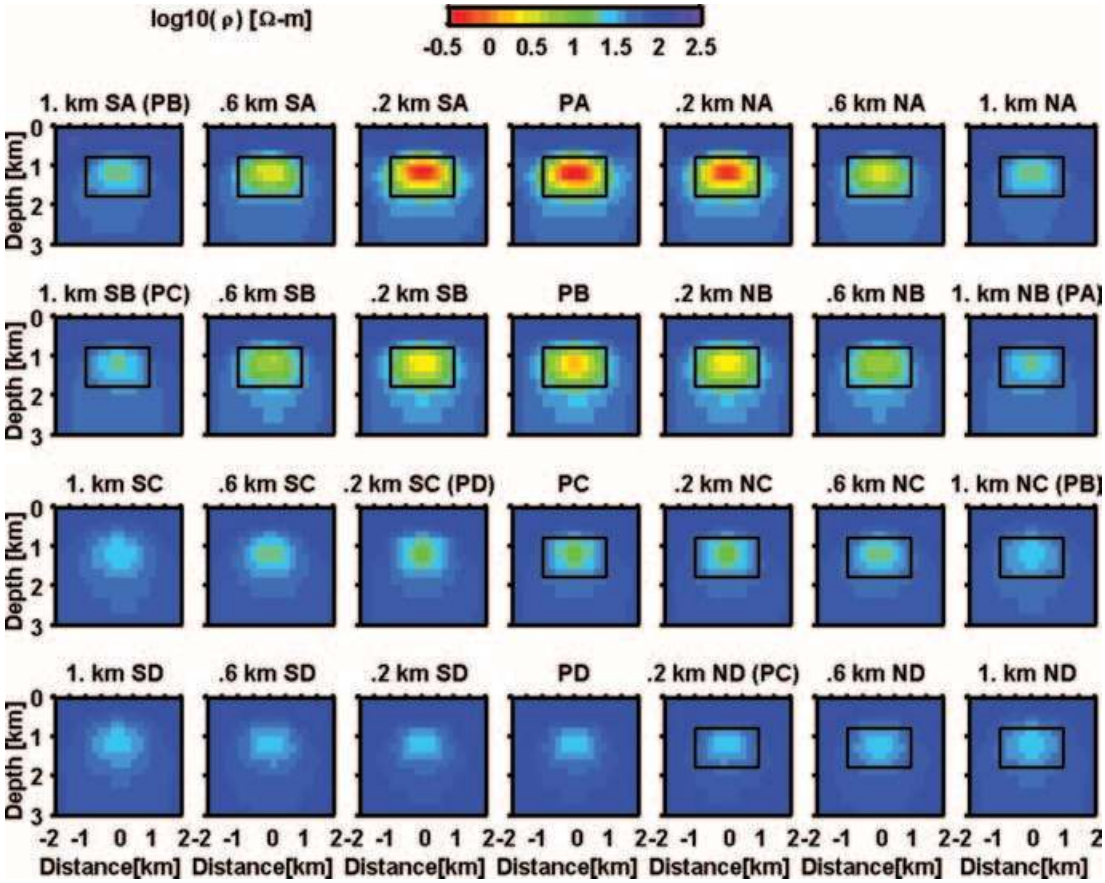

Figure 10. Resistivity cross-sections obtained by 3-D inversion of the off-diagonal tensor elements $\boldsymbol{Z}_{xy}$ and $\boldsymbol{Z}_{yx}$ generated for model BC. Plotting conventions are as in Fig. 8. Note that the model fit to the profile A data does not fit to the target level of 1 RMS.

better in some cases, as we have found it is possible to obtain a more reasonable (asymmetric) model similar to the full tensor inverse solutions for some starting models. But the off-diagonal terms by themselves cannot define the 'true' direction, so even if an asymmetric model fitting the data is found, off-profile structure will just as likely as not be imaged on the wrong side of the data profile. We conclude that interpretation of off-profile structure can be enhanced significantly by using all elements of the impedance tensor in the inversion.

4 CONCLUSIONS

Prior to 2-D inversion, it is necessary to identify a preferred geoelectrical strike. This is accomplished based on known local or regional geology or by performing some sort of dimensionality analysis on the data. Usually, the inferred geoelectrical strike varies over frequency, and over position on the profile. A compromise must usually be struck, and some data discarded or down-weighted so that 2-D inversion and interpretation can be justified. In some cases, e.g. for a single conductor exposed at the surface, inverting only TM mode data may yield a reasonable interpretation with minimal 3-D effects. However, not all structures are well resolved using only TM data, and in general the temptation is great to incorporate TE data in the interpretation. This data can easily be contaminated by 3-D effects, which are fitted by inserting spurious and misleading structure into the model.

By applying 3-D inversions to 2-D profile data, these potential problems can be minimized. In our examples the inversion produces reasonable results beneath the data. Although constraining the full 3-D structure would certainly require additional profiles, a single profile can provide at least a qualitatively reasonable picture of nearby off-profile structure. Much of the information about off-profile structure is contained in the diagonal elements $\boldsymbol{Z}_{xx}$ and $\boldsymbol{Z}_{yy}$, so 3-D inversion should include all tensor components if possible.

In this paper we have considered explicitly the case of a conductor buried in a more resistive host. Additional tests with a resistive body buried in a more conductive host were also conducted, with similar results, though the periods used in the inversion must be adjusted to cope with the shorter diffusion length scales of the electromagnetic fields in the host. We have not yet done tests with significantly more complex 3-D models. It is possible that if the local response is strongly affected by complex regional scale 3-D structure (e.g. near a complicated coastline) 3-D inversion of a single profile may conceivably still be misleading. Further research on this question is warranted.

ACKNOWLEDGMENTS

This research has been supported by a grant from the Thailand Research Fund (RSA4780021) to WS, and by DOE-

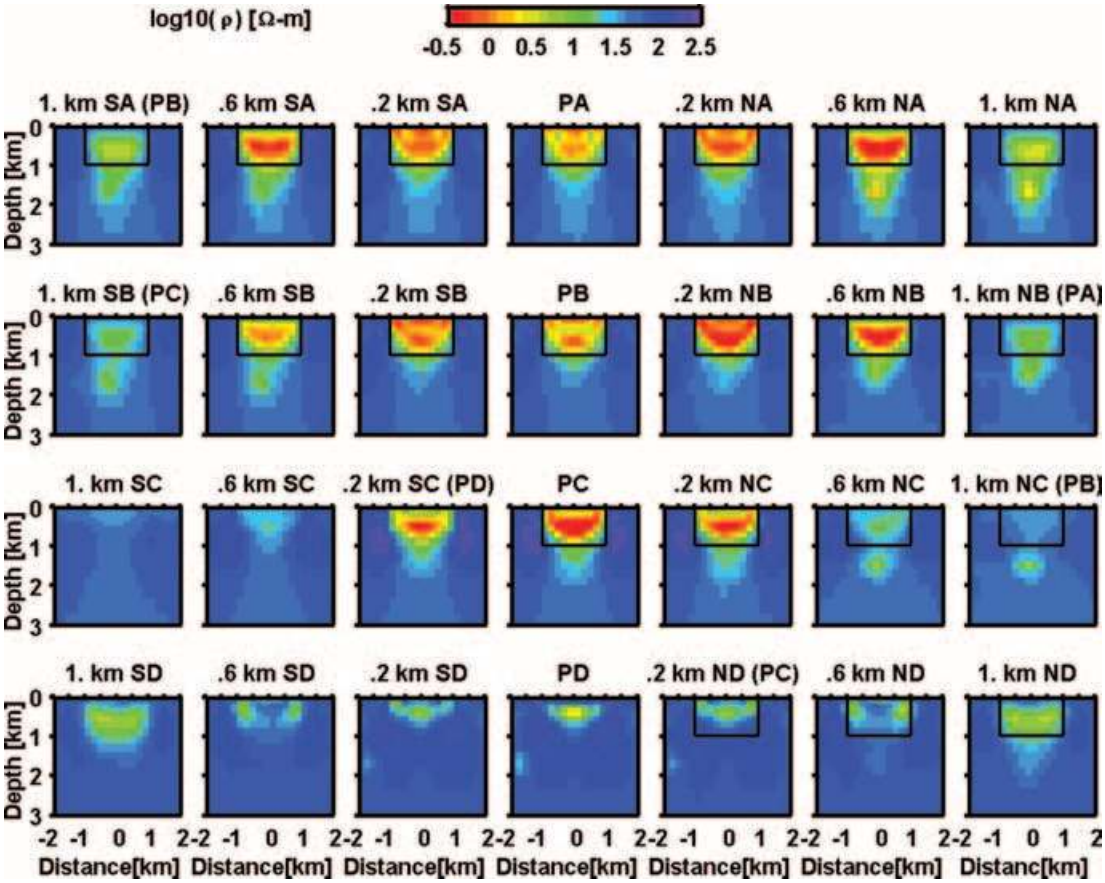

Figure 11. Resistivity cross-sections as in Fig. 10, obtained by inverting the off-diagonal tensor elements $\boldsymbol{Z}_{xy}$ and $\boldsymbol{Z}_{yx}$, but for model SC. Note that none of these models fit the data to within the target level of 1 RMS.

FG0302ER15318 to GE, and partly by a JSPS postdoctoral fellowships (P02053) and a grant from MEXT, Japan (02053) to WS and MU. The authors would like to thank Wolfgang Soyer and Graham Heinson for their suggestions for improving this manuscript.

REFERENCES

Bai, D. & Meju, M.A., 2003. Deep structure of the Longling-Ruili fault underneath Rulili basin near the eastern Himalayan syntaxis: insights from magnetotelluric imaging, *Tectonophysics,* **364,** 135–146.

Berdichevsky, M.N., Dmitriev, V.I. & Pozdnjakova, E.E., 1998. On two-dimensional interpretation of magnetotelluric soundings, *Geophys. J. Int.,* **133,** 585–606.

Bielinski, R.A., Park, S.K., Rybin, A., Batalev, V., Jun, S. & Sears, C., 2003. Lithospheric heterogeneity in the Kyrgyz Tien Shan imaged by magnetotelluric studies, *Geophys. Res. Lett.,* **30**(15), 1806, doi:10.1029/2003GL017455.

Brasse, H., Lezaeta, P., Rath, V., Schwalenberg, K., Soyer, W. & Haak, V., 2002. The Bolivian Altiplano conductivity anomaly, *J. geophys. Res.,* **107**(B5), 2096, doi:10.1029/2001JB000391.

Caldwell, T.G., Bibby, H. & Brown, C., 2004. The magnetotelluric phase tensor, *Geophys. J. Int.,* **158,** doi:10.1111/j.1365-246X.2004.02281.x.

Chave, A.D. & Smith, J.T., 1994. On electric and magnetic galvanic distortion tensor decompositions, *J. geophys. Res.,* **99,** 4669–4682.

Constable, C.S., Parker, R.L. & Constable, C.G., 1987. Occam's inversion: a practical algorithm for generating smooth models from electromagnetic sounding data, *Geophysics.,* **52,** 289–300.

deGroot-Hedlin, C. & Constable, S., 1990. Occam's inversion to generate smooth, two-dimensional models from magnetotelluric data, *Geophysics,* **55,** 1613–1624.

Groom, R.W. & Bailey, R., 1989. Decomposition of magnetotelluric impedance tensors in the presence of local three-dimensional galvanic distortion, *J. geophys. Res.,* **94,** 1913–1925.

Ledo, J., Queralt, P., Marti, A. & Jones, A.G., 2002. Two-dimensional interpretation of three-dimensional magnetotelluric data: an example of limitations and resolution, *Geophys. J. Int.,* **150,** 127–139.

Mitsuhata, Y., Ogawa, Y., Mishina, M., Kono, T., Yokokura, T. & Uchida, T., 2001. Electromagnetic heterogeneity of the seismogenic region of 1962 M6.5 Northern Miyagi Earthquake, northeastern Japan, *Geophys. Res. Lett.,* **28,** 4371–4374.

Ogawa, Y. & Uchida, T., 1996. A two-dimensional magnetotelluric inversion assuming Gaussian static shift, *Geophys. J. Int.,* **126,** 69–76.

Ogawa, Y. *et al.,* 2001. Magnetotelluric imaging of fluids in intraplate earthquakes zones, NE Japan back arc, *Geophys. Res. Lett.,* **28,** 3741–3744.

Parkinson, W.D., 1959. Directions of rapid geomagnetic fluctuations, *Geophys. J. R. astr. Soc.,* **2,** 1–14.

Pous, J., Heise, W., Schnegg, P., Munoz, G., Marti, J. & Soriano, C., 2002. Magnetotelluric study of the Las Canadas caldera (Tenerife, Canary Islands): structural and hydrogeological implications, *Earth planet. Sci. Lett.,* **204,** 249–263.

Rodi, W.L. & Mackie, R.L., 2001. Nonlinear conjugate gradients algorithm for 2-D magnetotelluric inversion, *Geophysics,* **66,** 174–187.

Sakkas, V., Meju, M.A., Khan, M.A., Haak, V. & Simpson, F., 2002. Magnetotelluric images of the crustal structure of Chyulu Hills volcanic field, Kenya, *Tectonophysics,* **346,** 169–185.

Siripunvaraporn, W. & Egbert, G., 2000. An efficient data-subspace inversion method for 2-D magnetotelluric data, *Geophysics*, **65,** 791–803.

Siripunvaraporn, W., Egbert, G. & Lenbury, Y., 2002. Numerical accuracy of magnetotelluric modeling: a comparison of finite difference approximations, *Earth Planets Space,* **54,** 721–725.

Siripunvaraporn, W., Egbert, G., Lenbury, Y. & Uyeshima, M., 2004. Three-dimensional magnetotelluric inversion: data space method, *Phys. Earth planet. Inter.,* doi:10.1016/j.pepi.2004.08.023

Smith, J.T. & Booker, J.R., 1991. Rapid inversion of two- and three-dimensional magnetotelluric data, *J. geophys. Res.,* **96,** 3905–3922.

Swift, C.M., 1967. A magnetotelluric investigation of electrical conductivity anomaly in the southwestern United States, *PhD thesis,* MIT, Cambridge, MA.

Unsworth, M., Bedrosian, P., Eisel, M., Egbert, G. & Siripunvaraporn, W., 2000. Along strike variations in the electrical structure of the San Andreas Fault at Parkfield, California, *Geophys. Res. Lett.,* **27,** 3021–3024.

Vozoff, K., 1972. The magnetotelluric method in the exploration of sedimentary basins, *Geophysics,* **37,** 98–141.

Wanamaker, P.E., Hohmann, G.W. & Ward, S.H., 1984. Magnetotelluric responses of three-dimensional bodies in layered earths, *Geophysics,* **49,** 1517–1533.

Wu, X., Ferguson, I.J. & Jones, A.G., 2002. Magnetotelluric response and geoelectric structure of the Great Slave Lake shear zone, *Earth planet. Sci. Lett.,* **196,** 35–50.